Available online at www.sciencedirect.com
ScienceDirect
Aerospace Science and Technology ••• (••••) •••–•••
Aerospace Science and Technology
www.elsevier.com/locate/aescte

A dual-wheel multi-mode spacecraft actuator for near-minimum-time large angle slew maneuvers

Willem H. Steyn *

Department of Electrical and Electronic Engineering, University of Stellenbosch, Stellenbosch 7600, South Africa

Received 22 February 2007; received in revised form 5 September 2007; accepted 17 January 2008

Abstract

A novel implementation of a dual-wheel actuator is presented for a spacecraft with high agility requirements, e.g. where the imaging payload is strapped to the satellite body and the bore sight has to be shifted from one target location to another by slewing the complete satellite in minimum-time. To maximise the torque capability, the actuator can be utilised as a "scissored" type control moment gyro (CMG-mode) with parallel gimbals. A system with 2 single-gimbal CMGs per body axis, can simplify the gimbal steering method with gimbal angle constraints and avoid any control torque singularities prevalent in other CMG configurations. During fine pointing maneuvers the dual-wheel actuator can be used in reaction wheel mode (RW-mode). In this way the unique advantages of both CMG and reaction wheel actuators can be exploited, while the transition between either modes can be done smoothly.

In CMG-mode the torque capability can be at least one order of magnitude greater and the peak electrical power requirement will be much lower during the CMG high torque phases of a maneuver, compared to the RW-mode. In RW-mode the torque resolution and wheel induced disturbances can be more conducive for the high stability requirement of an imaging payload. The dual-wheel units can be aligned and parked into two orthogonal axes during reaction wheel use, resulting in multiple redundancy, i.e. any two wheels may fail, while still maintaining full 3-axis control authority.

The paper will present the torque, angular momentum and gimbal steering equations for the dual-wheel actuator. Next, a near-minimum-time eigenaxis slew maneuver algorithm is derived for the CMG-mode, where optimal agility is required. Finally, the paper concludes with a simulation of a practical satellite application. The performance of a near-minimum-time eigenaxis slew maneuver in CMG-mode is compared to the results obtained when the maneuver is executed using a pyramid array of four single-gimbal CMGs with similar performance constraints and driven by time optimised, singularity robust steering logic.

Keywords: Control Moment Gyro; Minimum-time maneuvers; Singularity avoidance; Eigenaxis slew; Satellite attitude control

1. Introduction

Large angle slew maneuvers in minimum-time are often required for remote sensing satellites with strap down imaging payloads. High agility will increase the imaging opportunities for these spacecraft as many ground targets can be scanned within a short period of time, due to a reduction in the slew time between widely separated target locations. Slew maneuvers in minimum-time are driven by the torque and angular momentum capability of the attitude actuator and by the control algorithm used. For maximum torque a reaction control system (thrusters) can be used, but at the expense of propellant. Another more attractive option will be to use an angular momentum exchange system, requiring only electrical power. A specific type of actuator in this category with large torque capability is a CMG, where a momentum wheel running at a high angular speed is gimballed and rotated at a certain gimbal rate. The torque produced is then directly proportional to the cross product of the angular momentum vector and the gimbal rate vector. Another advantage of this type of actuator is also a much lower peak power requirement, compared to a reaction wheel system [5].

The dual-wheel implementation presented in this paper is based on a scissored-pair CMG with parallel gimbal axes.

* Tel.: +27 21 8084926; fax: +27 21 8084981.
E-mail address: whsteyn@sun.ac.za.

1270-9638/$ – see front matter © 2008 Published by Elsevier Masson SAS.
doi:10.1016/j.ast.2008.01.003

The use of scissored CMG pairs was first presented by Crenshaw [4], to produce a system relatively insensitive to singularity problems. Thomas and Paluszek [9] utilised a scissored-pair CMG with parallel gimbal axes per rotational joint of a multi-body robotic system to give singularity-free, reactionless slewing of a multi-joint robotic arm.

Various control algorithms for stable large angle slew maneuvers have been presented in the open literature, but not all succeeded to do the maneuver in minimum-time as well. Wie et al. [15] proposed a linear quaternion feedback (Q-feedback) regulator with decoupling for the gyroscopic torques to ensure an eigenaxis rotation (shortest angular path). Their Q-feedback controller assumes no actuator torque or angular momentum constraints. The slew maneuver will deviate from the eigenaxis when the actuators saturate on any of these constraints. Due to the Q-feedback controller's linear nature, it will not be minimum-time. Van der Bosch et al. [11] presented an adaptive control method to track a linear reference model for an eigenaxis rotation. The rotation time was not minimised, but the reaction wheel constraints were considered. Zwartbol et al. [16] presented a real time attitude generator for a principal axis, time optimal rotation trajectory. Although it is relatively simple to implement, only a single axis maneuver is possible.

Li and Bainum [6] describe an iterative numerical approach to find a minimum-time slew maneuver for a general rigid spacecraft. Bilimoria and Wie [1] presented a time-optimal three-axis reorientation controller for symmetric rigid spacecraft. The time-optimal maneuver will not necessarily be an eigenaxis rotation. Reductions in the slew time of a symmetric body compared to minimum-time eigenaxis rotations, were less than 10% for 180° maneuvers at the expense of a substantial increase in control torque. Byers and Vadali [2] extended the time-optimal reorientation problem to non-symmetric rigid bodies, by presenting approximate solutions to the optimal switching times. A feedforward/feedback control law to approximate the time-optimal solution in the presence of modelling errors, caused by gyroscopic coupling terms and moment of inertia differences, was proposed. The algorithms in [1] and [2] are computationally very demanding, marginally faster than pure eigenaxis rotations at the expense of a substantial increase in control energy.

Crassidis et al. [3] and Vadali [10] used variable structure control theory to implement robust large angle maneuvers. Although not time optimal, the maneuvers were robust against modelling errors and disturbance torques. Steyn [8] proposed a near-minimum-time (NMT) eigenaxis rotation controller using reaction wheels. The controller provides for wheel torque and angular momentum saturation. Although the controller computes the reaction wheel control torque in an open-loop manner, it uses feedback from the quaternion error to determine the half-way mark (mid-point). A simple feedback reference rate controller can be added to compensate for moment of inertia mismatches and to ensure convergence robustness for an eigenaxis rotation. Verbin and Ben-Asher [12] presented time efficient closed loop steering laws for rigid spacecraft doing large angle maneuvers. Their controllers are derived for three or four reaction wheels and address the wheel limiting constraints, i.e. maximum controller bandwidth for stability, maximum angular acceleration and maximum angular rate. A switching line method is used to satisfy the angular acceleration and rate limits. The controller will give an eigenaxis rotation and smooth switching from saturation to linear control at small angles.

The dual-wheel actuator presented next is ideally suited for minimum-time maneuvers when used in CMG-mode, due to its high torque capability. The NMT eigenaxis rotation controller presented in [8] for reaction wheels, is expanded in Section 3 for a dual-wheel system, where scissored-pair CMGs are used per body axis. The main difference is in the constraints: Torque and angular momentum saturation limit the control output when reaction wheels are used, while gimbal angle (for singularity avoidance) and gimbal angular rate, limit the maximum control output levels achievable in the CMG-mode. The paper concludes with simulation results in Section 4, comparing the expected large angle slew performance of the dual-wheel actuator in CMG-mode when using the expanded NMT controller to a pyramid array of four single-gimbal CMGs with similar constraints to the dual-wheel actuator (without gimbal angle limits), while driven by time optimised, singularity robust steering logic.

2. Dual-wheel actuator

A novel CMG and reaction wheel actuator for satellites, based on a scissored-pair dual-wheel arrangement with parallel gimbals, is shown in Fig. 1. An actuator is aligned along each principal body axis of the satellite to provide full 3-axis control authority. The X-axis actuator consists of two reaction/momentum wheels each mounted on a gimbal to rotate the momentum vectors $\mathbf{h}_{xa}$ and $\mathbf{h}_{xb}$ through an equal but opposite rotating angle δ_z in the XY-plane. In RW-wheel mode the gimbal angles $\pm\delta_z$ are zeroed and when wheel A increase its angular momentum by $\frac{1}{2}\Delta h_x$, wheel B will decrease its angular momentum by an equal value for a total momentum change of Δh_x. Any constant momentum bias h_0 in both wheels are completely cancelled at zero gimbal angle, but will result in a Y-axis momentum component at non-zero gimbal angle. The momentum bias components are also producing a control mo-

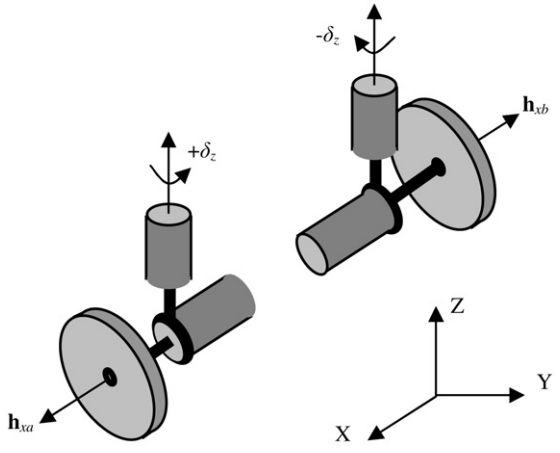

Fig. 1. X-axis dual-wheel actuator for CMG or RW use.

Please cite this article in press as: W.H. Steyn, A dual-wheel multi-mode spacecraft actuator for near-minimum-time large angle slew maneuvers, Aerospace Science and Technology (2008), doi:10.1016/j.ast.2008.01.003

ment gyroscopic torque vector aligned with the Y-axis for all gimbal angles less than ±90°.

To summarise: The dual-wheel X-axis actuator can be used as a X-axis reaction wheel at twice the momentum and torque capability of a single wheel. The dual-wheel X-axis actuator can also be used as a CMG with a resultant momentum and torque vector along the Y-axis.

From Fig. 1 the X-axis actuator produces an angular momentum vector,

$$\begin{aligned}\mathbf{h}_{xab} &= \left[(h_0 + \Delta h_x/2)\cos\delta_z - (h_0 - \Delta h_x/2)\cos\delta_z\right]\mathbf{x} \\ &\quad + \left[(h_0 + \Delta h_x/2)\sin\delta_z + (h_0 - \Delta h_x/2)\sin\delta_z\right]\mathbf{y} \\ &= [\Delta h_x \cos\delta_z]\mathbf{x} + [2h_0 \sin\delta_z]\mathbf{y} \end{aligned} \tag{1a}$$

and a torque vector,

$$\begin{aligned}\frac{\mathrm{d}}{\mathrm{d}t}(\mathbf{h}_{xab}) &= \left[\frac{\mathrm{d}}{\mathrm{d}t}(\Delta h_x)\cos\delta_z - \frac{\mathrm{d}}{\mathrm{d}t}(\delta_z)\Delta h_x \sin\delta_z\right]\mathbf{x} \\ &\quad + \left[\frac{\mathrm{d}}{\mathrm{d}t}(\delta_z)2h_0\cos\delta_z\right]\mathbf{y} \\ &= N_{rw\text{-}x}\mathbf{x} + N_{cmg\text{-}y}\mathbf{y} \end{aligned} \tag{1b}$$

Likewise, a Y-axis and Z-axis actuator, will produce,

$$\begin{aligned}\mathbf{h}_{yab} &= [\Delta h_y \cos\delta_x]\mathbf{y} + [2h_0 \sin\delta_x]\mathbf{z} \\ \frac{\mathrm{d}}{\mathrm{d}t}(\mathbf{h}_{yab}) &= \left[\frac{\mathrm{d}}{\mathrm{d}t}(\Delta h_y)\cos\delta_x - \frac{\mathrm{d}}{\mathrm{d}t}(\delta_x)\Delta h_y \sin\delta_x\right]\mathbf{y} \\ &\quad + \left[\frac{\mathrm{d}}{\mathrm{d}t}(\delta_x)2h_0\cos\delta_x\right]\mathbf{z} \\ &= N_{rw\text{-}y}\mathbf{y} + N_{cmg\text{-}z}\mathbf{z} \end{aligned} \tag{2}$$

and,

$$\begin{aligned}\mathbf{h}_{zab} &= [\Delta h_z \cos\delta_y]\mathbf{z} + [2h_0 \sin\delta_y]\mathbf{x} \\ \frac{\mathrm{d}}{\mathrm{d}t}(\mathbf{h}_{zab}) &= \left[\frac{\mathrm{d}}{\mathrm{d}t}(\Delta h_z)\cos\delta_y - \frac{\mathrm{d}}{\mathrm{d}t}(\delta_y)\Delta h_z \sin\delta_y\right]\mathbf{z} \\ &\quad + \left[\frac{\mathrm{d}}{\mathrm{d}t}(\delta_y)2h_0\cos\delta_y\right]\mathbf{x} \\ &= N_{rw\text{-}z}\mathbf{z} + N_{cmg\text{-}x}\mathbf{x} \end{aligned} \tag{3}$$

In RW-mode the gimbals will be parked at zero δ_i angles and the resultant reaction wheel angular momentum and torque vector on the satellite will be,

$$\mathbf{h}_{rw} = \begin{bmatrix}\Delta h_x \\ \Delta h_y \\ \Delta h_z\end{bmatrix}, \qquad \mathbf{N}_{rw} = \frac{\mathrm{d}}{\mathrm{d}t}(\mathbf{h}_{rw}) = \begin{bmatrix}\frac{\mathrm{d}}{\mathrm{d}t}(\Delta h_x) \\ \frac{\mathrm{d}}{\mathrm{d}t}(\Delta h_y) \\ \frac{\mathrm{d}}{\mathrm{d}t}(\Delta h_z)\end{bmatrix} \tag{4}$$

In CMG-mode the angular momentum on the wheels will be held constant at the bias value of h_0 per wheel. The resultant CMG angular momentum and torque vector will be,

$$\begin{aligned}\mathbf{h}_{cmg} &= \begin{bmatrix}2h_0\sin\delta_y \\ 2h_0\sin\delta_z \\ 2h_0\sin\delta_x\end{bmatrix}, \\ \mathbf{N}_{cmg} &= \frac{\mathrm{d}}{\mathrm{d}t}(\mathbf{h}_{cmg}) = \begin{bmatrix}\frac{\mathrm{d}}{\mathrm{d}t}(\delta_y)2h_0\cos\delta_y \\ \frac{\mathrm{d}}{\mathrm{d}t}(\delta_z)2h_0\cos\delta_z \\ \frac{\mathrm{d}}{\mathrm{d}t}(\delta_x)2h_0\cos\delta_x\end{bmatrix} \end{aligned} \tag{5}$$

During normal attitude control operations e.g. fine pointing and target tracking, the satellite will be in RW-mode. External torque disturbances may lead to a small buildup in angular momentum ($\Delta h_i \neq 0$). With a continuous momentum dumping procedure (using magnetic torquers or thrusters) the buildup value can be contained to small values, i.e. a few orders of magnitude smaller than the momentum bias value h_0.

For agility during large angle slew maneuvers the dual-wheel actuators will be used in CMG-mode due to a much larger torque capability and much lower electrical peak power requirement, compared to the RW-mode. In CMG-mode the gimbal actuator has to rotate the momentum wheel at a low angular rate, while maintaining a constant speed on the momentum wheel. In RW-mode the wheel actuators have to produce maximum torque (high drive motor current) at high wheel angular rates (high drive motor voltage) resulting in a large electrical power requirement.

From Eqs. (1) to (3): If the reaction wheel angular momentum has not been dumped fully to zero before the CMG-mode is entered, a small CMG disturbance torque vector can be generated,

$$\mathbf{N}_{cmg\_distb} = \begin{bmatrix}-\frac{\mathrm{d}}{\mathrm{d}t}(\delta_z)\Delta h_x \sin\delta_z \\ -\frac{\mathrm{d}}{\mathrm{d}t}(\delta_x)\Delta h_y \sin\delta_x \\ -\frac{\mathrm{d}}{\mathrm{d}t}(\delta_y)\Delta h_z \sin\delta_y\end{bmatrix} \tag{6}$$

This disturbance torque vector (6) contribution is much less (see discussion below) than the ideal CMG torque vector (5) when the gimbal angles are prevented from approaching a torque and angular momentum singularity at ±90° (e.g. when limited to maximum excursion angles of ±75°, the CMG torque capability has been reduced to 26% of its maximum value at the zero gimbal angle and the CMG momentum capability reached 97% of the theoretical maximum of $2h_0$ at ±90°). However, the disturbance torque vector is also a known quantity and can easily be accounted for when the required gimbal steering rate vector is computed from the required control torque vector,

$$\begin{aligned}\mathbf{N}_{control} &= \mathbf{N}_{cmg} + \mathbf{N}_{cmg\_distb} \\ &= \begin{bmatrix}0 & 2h_0\cos\delta_y & -\Delta h_x\sin\delta_z \\ -\Delta h_y\sin\delta_x & 0 & 2h_0\cos\delta_z \\ 2h_0\cos\delta_x & -\Delta h_z\sin\delta_y & 0\end{bmatrix} \\ &\quad \times \begin{bmatrix}\frac{\mathrm{d}}{\mathrm{d}t}(\delta_x) \\ \frac{\mathrm{d}}{\mathrm{d}t}(\delta_y) \\ \frac{\mathrm{d}}{\mathrm{d}t}(\delta_z)\end{bmatrix} \end{aligned} \tag{7a}$$

or,

$$\begin{aligned}&\begin{bmatrix}\frac{\mathrm{d}}{\mathrm{d}t}(\delta_x) \\ \frac{\mathrm{d}}{\mathrm{d}t}(\delta_y) \\ \frac{\mathrm{d}}{\mathrm{d}t}(\delta_z)\end{bmatrix} \\ &= \begin{bmatrix}\frac{\Delta h_z\tan\delta_y}{4h_0^2\cos\delta_x} & \frac{\Delta h_x\Delta h_z\tan\delta_y\tan\delta_z}{8h_0^3\cos\delta_x} & \frac{1}{2h_0\cos\delta_x} \\ \frac{1}{2h_0\cos\delta_y} & \frac{\Delta h_x\tan\delta_z}{4h_0^2\cos\delta_y} & \frac{\Delta h_x\Delta h_y\tan\delta_x\tan\delta_z}{8h_0^3\cos\delta_y} \\ \frac{\Delta h_y\Delta h_z\tan\delta_x\tan\delta_y}{8h_0^3\cos\delta_z} & \frac{1}{2h_0\cos\delta_z} & \frac{\Delta h_y\tan\delta_x}{4h_0^2\cos\delta_z}\end{bmatrix}\mathbf{N}_{control} \end{aligned} \tag{7b}$$

Please cite this article in press as: W.H. Steyn, A dual-wheel multi-mode spacecraft actuator for near-minimum-time large angle slew maneuvers, Aerospace Science and Technology (2008), doi:10.1016/j.ast.2008.01.003

It can be seen from (7b) that a steering rate vector exist, with all required gimbal rate components deviating by less than 20% from a simplified solution of (5), if all gimbal angles are limited $|\delta_i| < 75°$ and all $|\Delta h_i| < 0.1h_0$.

3. CMG-mode near-minimum-time (NMT) eigenaxis slew

A previous paper [8] presents a NMT eigenaxis rotation control technique, using reaction wheels. This algorithm is expanded in this paper for use during the CMG-mode of the dual-wheel actuators. To avoid copying all the detail in the previous paper, only the essential equations will be repeated to enable the reader to follow the derivation of the expanded algorithm for CMG use.

If we assume we have an earth observation satellite in a LEO near-circular orbit, it is convenient to define the attitude with respect to the orbit reference coordinates (ORC). The spacecraft body coordinates (SBC) will then be aligned to the orbit axes when the Z-body axis is nadir pointing, the Y-body axis is anti-normal to the orbit plane and the X-body axis is in the flight direction. An eigenaxis slew will then have a fixed rotation axis (Euler vector $\mathbf{e} = [e_{xo} \quad e_{yo} \quad e_{zo}]^T$) with respect to the ORC. Then, for the vector components of the error quaternion $\mathbf{q}_e = [q_{1e} \quad q_{2e} \quad q_{3e} \quad q_{4e}]^T$,

$$\frac{q_{ie}(t)}{q_{je}(t)} = \text{const} \quad i, j = 1, 2, 3 \; \forall i \neq j \tag{8}$$

Likewise, during the eigenaxis maneuver the angular body rate vector (orbit referenced) will point in the same fixed direction as the Euler axis:

$$\boldsymbol{\omega}_B^O = [\,\omega_{xo} \quad \omega_{yo} \quad \omega_{zo}\,]^T = \left[e_{xo}\frac{\mathrm{d}}{\mathrm{d}t}(\Phi) \quad e_{yo}\frac{\mathrm{d}}{\mathrm{d}t}(\Phi) \quad e_{zo}\frac{\mathrm{d}}{\mathrm{d}t}(\Phi) \right]^T \tag{9}$$

with,

$\Phi =$ Euler rotation angle, therefore

$$\frac{\omega_{io}(t)}{\omega_{jo}(t)} = \text{const} \quad i, j = x, y, z \; \forall i \neq j \tag{10}$$

If we assume relatively small gyroscopic, gravity gradient and other disturbance torques compared to the large CMG torque during a slew maneuver, a near-minimum-time eigenaxis rotation will be possible. Minimum-time rotations will only be possible if all the other torques mentioned above are exactly zero and the maximum available CMG torque can be applied to the eigenaxis slew. From (5) the maximum CMG torque will be time varying as a cosine function of the gimbal angles and will peak at the maximum allowable gimbal rate. If the CMG gimbals start at zero angle at the beginning of the eigenaxis rotation, the CMG torque will also be maximum and as the gimbals rotate (gimbal angles increase) the torque will reduce due to the cosine relationship, until the gimbal angle limit is encountered.

At the gimbal angle limit the gimbal rate must be zeroed and the CMG torque will become zero. The minimum-time slew maneuver will therefore typically execute as a Bang-Off-Bang sequence: Initially a maximum CMG torque at maximum gimbal rate will accelerate the rotation angle $\Phi(t)$ as the satellite slews, then the satellite will start to coast at a constant rotation rate when the gimbal angle limit is encountered. Finally a maximum opposite CMG torque profile will decelerate the rotation angle, until the full maneuver is completed. The Euler angle acceleration profile (see Fig. 2) can be implemented as,

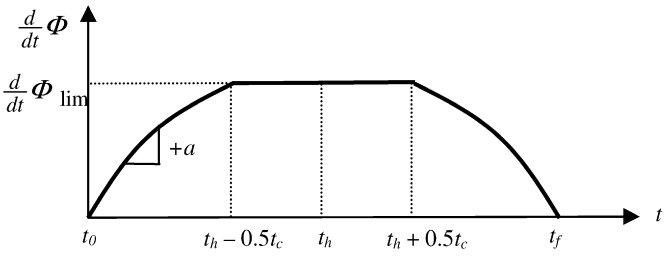

Fig. 2. Euler angular rate profile during a minimum-time slew maneuver.

$$\frac{\mathrm{d}^2}{\mathrm{d}t}(\Phi) = \begin{cases} +a\{\delta(t)\} & \{t \in t_0, t_h - 0.5t_c\} \\ 0 & \{t \in t_h - 0.5t_c, t_h + 0.5t_c\} \\ -a\{\delta(t)\} & \{t \in t_h + 0.5t_c, t_f\} \end{cases} \tag{11}$$

where,

$\pm a\{\delta(t)\} =$ Acceleration/deceleration profile

$t_h =$ Time at halfway mark

$t_c =$ Time period to coast at gimbal angle limit

$t_f =$ Time at completion of slew

If the required slew angle is less than a certain value, the gimbal angle limit may not be reached and the coast period will be zero. The time when the halfway mark is reached will be determined during the maneuver by comparing the largest error quaternion component to its pre-computed value q_{half} at the halfway mark:

$$\max_i |q_{ie}(t)| - q_{half} = \begin{cases} > 0 & \forall t < t_h \\ < 0 & \forall t > t_h \end{cases} \quad i = 1, 2, 3 \tag{12}$$

where,

$$q_{half} = \frac{\max_i |q_{ie}(t_0)|}{|\sin(\Phi/2)|} \left|\sin(\Phi/4)\right| \tag{13}$$

From (9) it is clear that the angular body rates ω_{xo}, ω_{yo} and ω_{zo} will have a similar profile to Fig. 2, but scaled with the Euler vector components. To obtain a maximum gradient profile for a minimum-time eigenaxis slew, the maximum gimbal rate must be maintained throughout the acceleration and deceleration phases. To provide for an additional torque capacity to compensate for the small gravity gradient, gyroscopic and other known disturbance torques (to enable "uncoupled" dynamics within ORC), a NMT eigenaxis slew will be implemented by backing off slightly from the maximum gimbal rate. The "uncoupled" orbit referenced dynamics can be obtained in the following way: The spacecraft dynamics in inertial space can be described by the Euler equation,

$$\mathbf{I}\dot{\boldsymbol{\omega}}_B^I = \mathbf{N}_{gg} + \mathbf{N}_{gyro} - \mathbf{N}_{cmg} + \mathbf{N}_d \tag{14}$$

where,

Please cite this article in press as: W.H. Steyn, A dual-wheel multi-mode spacecraft actuator for near-minimum-time large angle slew maneuvers, Aerospace Science and Technology (2008), doi:10.1016/j.ast.2008.01.003

$\mathbf{N}_{gg} = 3\omega_0^2[\mathbf{z}_0^B \times \mathbf{I}\mathbf{z}_0^B] =$ gravity gradient torque vector

$\mathbf{N}_{gyro} = -\boldsymbol{\omega}_B^I \times (\mathbf{I}\boldsymbol{\omega}_B^I + \mathbf{h}_{cmg}) =$ gyroscopic coupling

$\mathbf{N}_{cmg} = \dot{\mathbf{h}}_{cmg} =$ CMG generated torque vector, see (5)

Furthermore, $\boldsymbol{\omega}_B^I$ is the inertially referenced body angular rate vector, $\mathbf{I}$ is the inertia matrix, ω_0 is the orbit angular rate (almost constant for a near-circular orbit), $\mathbf{z}_0^B$ is the nadir unit vector in SBC and $\mathbf{N}_d$ is an unmodelled disturbance torque vector.

The ORC angular body rate vector can be determined from the inertially referenced body rate vector, using the attitude transformation matrix $\mathbf{A}$,

$$\boldsymbol{\omega}_B^O = \boldsymbol{\omega}_B^I - \mathbf{A}\,[0 \quad -\omega_0 \quad 0]^T = \boldsymbol{\omega}_B^I + \omega_0 \mathbf{A}_2 \tag{15}$$

Using Eqs. (14) and (15), the ORC dynamic equation,

$$\begin{aligned}\mathbf{I}\dot{\boldsymbol{\omega}}_B^O &= \mathbf{N}_{gg} + \mathbf{N}_{gyro} - \mathbf{N}_{cmg} + \mathbf{N}_d + \omega_0 \mathbf{I}\dot{\mathbf{A}}_2 \\ &= \mathbf{N}_{slew} + \mathbf{N}_d\end{aligned} \tag{16}$$

We can "uncouple" the spacecraft dynamics easily between body axes by compensating for the small additional torques (typically more than 2 orders of magnitude smaller than the required maximum CMG torque component during NMT slew maneuvers). The required CMG torque vector during a slew to give "uncoupled" dynamics is,

$$\mathbf{N}_{cmg} = \mathbf{N}_{add} - \mathbf{N}_{slew} \tag{17}$$

with,

$$\mathbf{N}_{add} = \mathbf{N}_{gg} + \mathbf{N}_{gyro} + \omega_0 \mathbf{I}\dot{\mathbf{A}}_2$$

For the uncoupled dynamics, ignoring the small $\mathbf{N}_d$ as insignificant compared to $\mathbf{N}_{slew}$ and assuming small products of inertia (body axes closely aligned to the principal axes) i.e. $\mathbf{I} = \text{diag}\{I_{xx}, I_{yy}, I_{zz}\}$, we have during the acceleration and deceleration phases of the slew maneuver.

$$\frac{I_{ii}\dot{\omega}_{io}}{I_{jj}\dot{\omega}_{jo}} = \left.\frac{N_{slew\text{-}i}}{N_{slew\text{-}j}}\right|_{accel/decel} = \text{const} \quad i, j = x, y, z \;\forall i \neq j \tag{18}$$

We already have, from (8) to (10), e.g. when $i = x$ and $j = y$ during an eigenaxis slew,

$$\omega_{xo}/\omega_{yo} = e_{xo}/e_{yo} = q_{1e}/q_{2e}$$

thus,

$$\left.\frac{N_{slew\text{-}x}}{N_{slew\text{-}y}}\right|_{accel/decel} = \frac{I_{xx} q_{1e}}{I_{yy} q_{2e}} \tag{19}$$

The relationship in (19) (all combinations of x, y, z and $q_{vec} = [q_{1e}, q_{2e}, q_{3e}]$) can now be used during the acceleration and deceleration phases of an eigenaxis slew to determine the respective components of the NMT slew torque vector,

$$\mathbf{N}_{slew} = \begin{cases} +s \min_i \left|\frac{N_{max\text{-}i}}{I_{ii} q_{ie}}\right| \text{diag}(\mathbf{I})\mathbf{q}_{vec} & t \in \{t_0, t_h - 0.5t_c\} \\ \mathbf{0} \quad t \in \{t_h - 0.5t_c, t_h + 0.5t_c\} \\ -s \min_i \left|\frac{N_{max\text{-}i}}{I_{ii} q_{ie}}\right| \text{diag}(\mathbf{I})\mathbf{q}_{vec} & t \in \{t_h + 0.5t_c, t_f\} \end{cases} \tag{20}$$

where,

$i =$ the body axis requiring the largest control effort

$s \in (0, 1) =$ the back-off fraction from the maximum available torque in axis i

$N_{max\text{-}i} =$ the maximum CMG torque possible in axis i (computed from (5) or (7) as a function of the gimbal angles and maximum allowed gimbal rate)

Depending on the amount of additional torque required to "uncouple" the dynamics of the Bang-Off-Bang slew maneuver between axes, an optimal value of s can be chosen (typically 0.9 to 0.95), resulting in a NMT eigenaxis slew. Although the slew torque (20) is computed in an open-loop manner, the halfway mark is determined using feedback from the error quaternion, see (12) and (13).

The full algorithm for a NMT eigenaxis rotation can now be summarised as follows:

1) Determine the initial error quaternion $\mathbf{q}_e(t_0)$ at the start of the slew maneuver.
2) Determine the spacecraft axis i of maximum eigenaxis control effort, from (19).
3) Determine the quaternion error component of axis i at the halfway mark, from (13).
4) Compute the corresponding near-maximum CMG slew torque vector, from (20).
5) Use the acceleration phase slew torques plus the additional torques (17) to compute the CMG torque vector and determine the required CMG gimbal rate vector, from (5) or (7).
6) Apply the gimbal rate vector command to the CMG by repeating step 5 until the halfway mark is reached (12), then go to step 9, else if a gimbal angle limit (typically 75°) is encountered, go to the next step.
7) Zero the required slew torque for the acceleration phase and allow the eigenaxis slew rotation to coast.
   Note: The additional torques for uncoupled dynamics are still applied and the CMG gimbal angles can still rotate slowly as a result of these small torques.
8) Repeat step 7 until an equal coasting period ($0.5t_c$) is completed before and after the halfway mark.
9) For the deceleration phase, use the slew torques from (20) plus additional torques to compute the CMG torque vector and gimbal rate vector.
10) Repeat step 9, until the absolute value of the reference slew rate vector $\boldsymbol{\omega}_{ref}^{\#}$ approaches zero*.

*Another approach will be to repeat the deceleration phase until the slew time $t = 2t_h = t_f$, but this may lead to larger attitude and angular rate errors at termination as a result of small differences in the acceleration and deceleration profile. These differences are mainly caused by the additional torques having an influence on the maximum CMG torque $N_{max\text{-}i}$ calculations (20), leading to small deviations in the symmetry of the gimbal angles between the respective phases.

Please cite this article in press as: W.H. Steyn, A dual-wheel multi-mode spacecraft actuator for near-minimum-time large angle slew maneuvers, Aerospace Science and Technology (2008), doi:10.1016/j.ast.2008.01.003

[#]The reference slew rate vector is determined by solving the "uncoupled" dynamic equation (16) during the eigenaxis slew maneuver,

$$\mathbf{I}\dot{\boldsymbol{\omega}}_{ref} = \mathbf{N}_{slew} \tag{21}$$

To compensate for any small attitude and/or rate errors at the completion of the eigenaxis Bang-Off-Bang maneuver due to unmodelled disturbances or small moment of inertia mismatches, a linear quaternion feedback regulator [15] will be used in the RW-mode,

$$\mathbf{N}_{control} = \mathbf{K}\mathbf{q}_{vec} + \mathbf{D}\boldsymbol{\omega}_B^O + \mathbf{N}_{add} \tag{22}$$

with,

$$\mathbf{K} = k\mathbf{I} \quad \text{and} \quad \mathbf{D} = d\mathbf{I} \quad (\mathbf{I} = \text{MOI matrix}) \quad \text{for}$$

a non-minimum-time globally stable eigenaxis rotation [15].

In case of larger moment of inertia (MOI) mismatches, greater deviations can occur from the eigenaxis during the NMT slew maneuver. A rate feedback compensation torque using the measured ORC angular rate vector and the reference angular rate vector as obtained from (21), can solve the problem of large MOI uncertainty,

$$\mathbf{N}_{comp} = \mathbf{C}\big[\boldsymbol{\omega}_B^O - \boldsymbol{\omega}_{ref}\big] \tag{23}$$

The compensation torque will be added to the CMG control torque (17) to keep the NMT slew maneuver close to the ideal eigenaxis rotation in spite of MOI uncertainty. It was shown in [8] that the feedback gain matrix $\mathbf{C}$ can be any diagonal positive matrix $\mathbf{C} = \text{diag}\{C_x,\ C_y,\ C_z\}$ larger than a certain minimum, for eigenaxis convergence. A sufficient condition will be [8],

$$\begin{aligned}
&C_x > \max\big\{|k_1\omega_{ref\text{-}y}|, |k_1\omega_{ref\text{-}z}|\big\}\\
&C_y > \max\big\{|k_2\omega_{ref\text{-}x}|, |k_2\omega_{ref\text{-}z}|\big\}, \quad \text{where}\\
&C_z > \max\big\{|k_3\omega_{ref\text{-}x}|, |k_3\omega_{ref\text{-}y}|\big\}\\
&k_1 = \Delta I_{yy} - \Delta I_{zz} \qquad k_2 = \Delta I_{zz} - \Delta I_{xx}\\
&k_3 = \Delta I_{xx} - \Delta I_{yy}\\
&\mathbf{I}_{true} = \text{diag}\{I_{xx} + \Delta I_{xx},\ I_{yy} + \Delta I_{yy},\ I_{zz} + \Delta I_{zz}\}
\end{aligned} \tag{24}$$

4. Simulation results

A minisatellite with an imaging payload will be fitted with the new dual-wheel actuator. Due to a large cylindrical optical payload fitted along the body Z-axis, the satellite MOI matrix is expected to be,

$$\mathbf{I} = \begin{bmatrix} 150 & 0 & 0 \\ 0 & 150 & 0 \\ 0 & 0 & 75 \end{bmatrix} \text{kg m}^2 \tag{25}$$

For best agility during large slew maneuvers, it will be best to use the dual-wheel actuator in CMG-mode and utilise a NMT eigenaxis rotation. The design parameters of the dual-wheel actuator are summarised in Table 1.

For comparison purposes a large angle slew maneuver is done, a) using the dual-wheel actuator in CMG-mode with a NMT eigenaxis procedure, and b) using a pyramid array of four single gimbal CMGs (4-SGCMG) with a singularity robust steering law. In both configurations the gimbal rate limitation of the CMGs is taken into account. A typical command at start of imaging will be to rotate the imager bore sight from the nominal nadir pointing attitude to a required off-track roll angle and to pitch the satellite ahead for a forward motion compensation maneuver. The yaw rotation around the bore sight will have to stay at zero during this pre-imaging slew. The roll, pitch and yaw reference vector (Euler 2-1-3 rotation) is therefore selected as,

$$\mathbf{RPY} = [30^\circ \quad 25^\circ \quad 0^\circ]^T \tag{26}$$

Table 1
Dual-wheel actuator parameters

CMG-mode	Nominal momentum $2h_0$	3 Nms
	Max gimbal rate $\dot{\delta}_{max}$	$\pm 16\,^\circ$/sec
	Max gimbal angle δ_{max}	$\pm 75^\circ$
	Max CMG torque $N_{cmg\text{-}max}$	± 0.84 Nm
RW-mode	Max momentum	± 3 Nms
	Max RW torque $N_{rw\text{-}max}$	± 0.1 Nm

All simulation results were produced in Matlab/SimuLink® using a complete model of the satellite's dynamics and kinematics. The body (inertially referenced) angular rate vector during the large angle maneuver is measured using a 3-axis fiber optic gyroscope (FOG) system. The attitude quaternion is accurately estimated during flight, utilising an extended Kalman filter (EKF) combining measurements from sun, earth and star sensors. During the large angle maneuver the attitude quaternion is propagated using the FOG measured body angular rate vector. This is done to prevent a reduction in estimated attitude accuracy due to the limited FOV of the attitude sensors and a decrease in measurement accuracy as a result of the high slew rates. The FOG measurement noise has a RMS value of 3.6 milli-deg/sec and is sampled at 10 Hz. All controllers presented in the simulation tests are also implemented at a discrete sampling frequency of 10 Hz. During all the simulation tests presented in this section the true (unknown) satellite MOI matrix was chosen as,

$$\mathbf{I}_{true} = \text{diag}\{148.0,\ 152.0,\ 75.0\}\ \text{kg m}^2 \tag{27}$$

4.1. Dual-wheel CMG-mode simulation

The gimbal angle limit used for entering the coast period t_c(11), between the acceleration and deceleration profiles of the eigenaxis slew, was chosen to be 95% of the maximum allowable gimbal angle, i.e. $\pm 71.25^\circ$. The back-off fraction (20) from the maximum allowable gimbal rate (maximum CMG torque), was chosen to be $s = 0.9$ (90% of $N_{max\text{-}i} = 0.756$ Nm, or 90% of $\dot{\delta}_{max} = \pm 14.4\,^\circ$/sec). These settings will allow for the additional torques (17) to be added to the CMG slew torque to "uncouple" the body axis dynamics during the eigenaxis rotation. The back-off settings will also give an additional margin to the CMG control torque for the compensation torque (23) to be added, to ensure a NMT slew maneuver (i.e. a fast eigenaxis rotation) in spite of MOI uncertainty.

Please cite this article in press as: W.H. Steyn, A dual-wheel multi-mode spacecraft actuator for near-minimum-time large angle slew maneuvers, Aerospace Science and Technology (2008), doi:10.1016/j.ast.2008.01.003

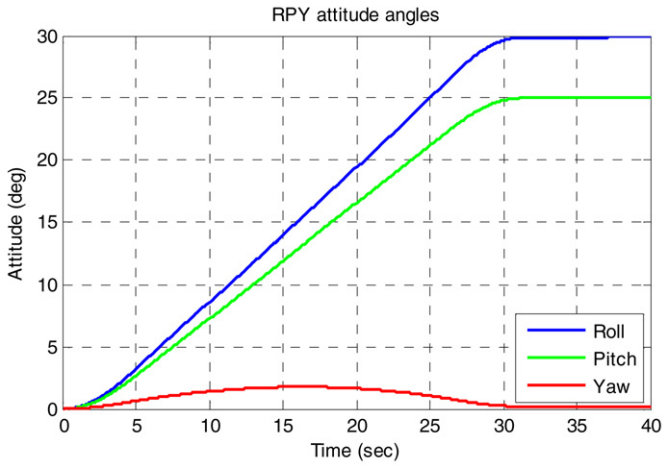

Fig. 3. NMT attitude angles in CMG-mode.

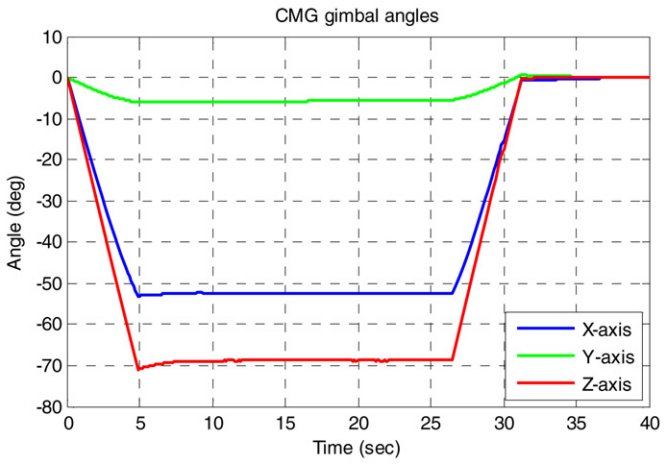

Fig. 5. CMG gimbal angles during NMT rotation.

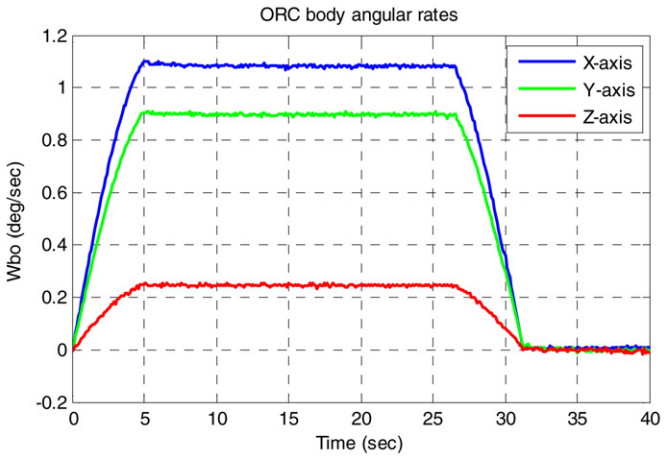

Fig. 4. NMT measured body rate vector in CMG-mode.

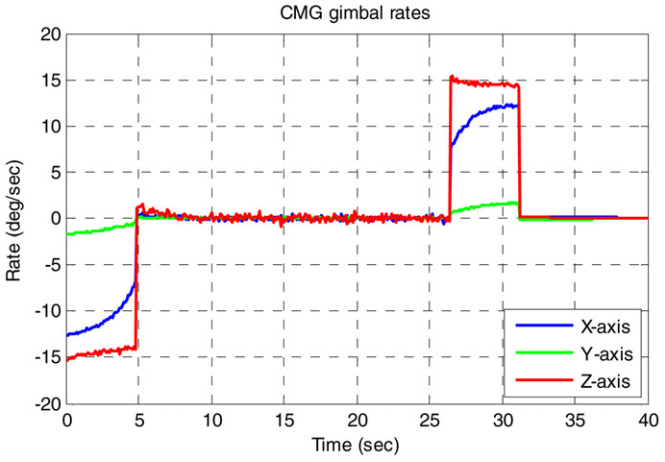

Fig. 6. CMG gimbal rates during NMT rotation.

The modelled MOI matrix $\mathbf{I}$ used in the Bang-Off-Bang control law (20) was chosen to be similar to (25). The feedback gain matrix for calculating the compensation torque (23) was selected to be, $\mathbf{C} = \text{diag}\{80.0,\ 80.0,\ 40.0\}$.

Figs. 3 to 8 present the results from a NMT slew in CMG-mode. Fig. 3 show how the attitude reference angles are reached in approximately 31 seconds using the Bang-Off-Bang optimum strategy. The ORC body angular rates in Fig. 4 show the symmetry of the 5 second acceleration phase, then the 21 second coasting phase and finally the 5 second deceleration phase. Fig. 5 shows how the gimbal angles perform with the Z-axis CMG unit, first reaching the 95% gimbal angle limit of $-71.25°$ after 5 seconds. Immediately thereafter, the coasting phase is entered and any further gimbal angle rotations are only due to the additional and compensation torques that are required. At the completion of the slew maneuver a small non-zero gimbal angle offset may be experienced. Typically, the CMG-mode will terminate immediately after the large angle slew maneuver and the attitude control will revert back to a RW-mode implementation of the quaternion feedback control law (22). The gimbal angles can then be zeroed, using a low constant gimbal rate command and the resulting small momentum disturbance will be effectively compensated for by the RW-mode quaternion feedback controller.

Fig. 6 presents the gimbal rates during the NMT slew. It can be seen how the gimbal rate of the CMG with largest control effort requirement (Z-axis), stays almost constant at the 90% limit of $\pm 14.4\,°/\text{sec}$ (the small deviations are due to the required additional and compensation torques). The X- and Y-axes gimbal rates are proportionally slower, as calculated from (7) and the required fixed ratios of the CMG slew torque vector components (18) to ensure an eigenaxis rotation (see Fig. 7). Fig. 8 shows the CMG angular momentum vector in spacecraft body coordinates. The angular momentum exchange between the CMGs and the satellite body is clear to see, by comparing Figs. 4 and 8.

4.2. *Pyramid 4-SGCMG simulation*

The performance of a typical 4-SGCMG pyramid configuration was also compared to the results obtained with the dual-wheel arrangement (six SGCMGs in three scissored-pairs). The SGCMGs in the pyramid shape are mounted with a skew angle $\beta = 30°$ to increase the torque and momentum saturation lev-

Please cite this article in press as: W.H. Steyn, A dual-wheel multi-mode spacecraft actuator for near-minimum-time large angle slew maneuvers, Aerospace Science and Technology (2008), doi:10.1016/j.ast.2008.01.003

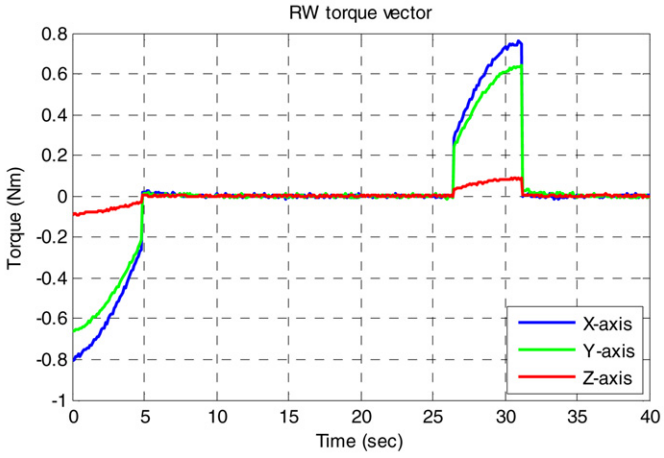

Fig. 7. Total CMG torque during NMT rotation.

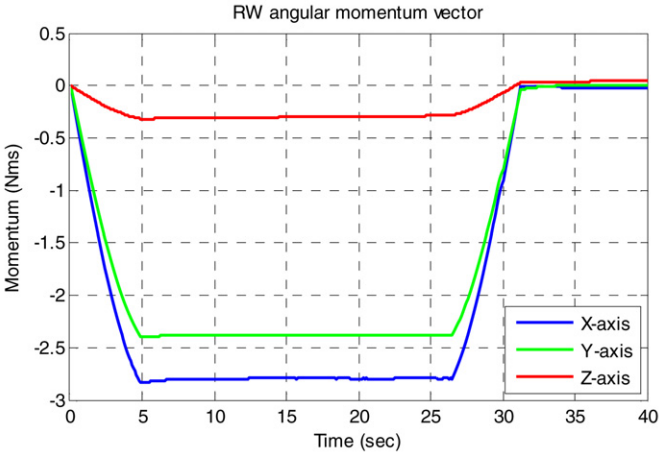

Fig. 8. CMG momentum vector during NMT rotation.

els in the body X- and Y-axes, due to the higher MOI values compared to the body Z-axis. The other SGCMG parameters are similar to those of the dual-wheel presented in Table 1, i.e. $h_0 = 1.5$ Nms per SGCMG and $\dot{\delta}_{max} = \pm 16\,^\circ$/sec. For a fair comparison to the CMG-mode implementation a limit of 93.75% $\dot{\delta}_{max} = \dot{\delta}_{\lim} = \pm 15.0\,^\circ$/sec was enforced on the maximum gimbal rates. No gimbal angle constraint was assumed (as is normally done for SGCMG configurations).

The CMG steering law utilised, is the generalised singularity robust (GSR) pseudo-inverse logic of Wie et al. [14] where,

$$\dot{\boldsymbol{\delta}} = \mathbf{A}^{\#}\mathbf{N}_{cmg} \quad \text{with } \mathbf{A}^{\#} = \mathbf{A}^T\left[\mathbf{A}\mathbf{A}^T + \lambda\mathbf{E}\right]^{-1}$$
$$\lambda = 0.2\exp\left[-\mathbf{A}\mathbf{A}^T\right], \quad \mathbf{E} = \begin{bmatrix} 1 & \varepsilon_3 & \varepsilon_2 \\ \varepsilon_3 & 1 & \varepsilon_1 \\ \varepsilon_2 & \varepsilon_1 & 1 \end{bmatrix} \tag{28}$$
$$\varepsilon_\iota = 0.1\sin(0.5\pi t + \phi_i) \quad \text{with } \phi_1 = 0,\ \phi_2 = 0.5\pi,\ \phi_3 = \pi$$

The required 4-SGCMG control torque $\mathbf{N}_{cmg}$ is calculated from the quaternion feedback control law with variable limiter as proposed by [14] for agile spacecraft:

$$\mathbf{N}_{cmg} = \mathbf{K}\operatorname*{sat}_{L_i}(\mathbf{q}_{vec}) + \mathbf{D}\boldsymbol{\omega}_B^O + \mathbf{N}_{add} \tag{29}$$
$$L_i = (d/k)\min\left\{\sqrt{4a_i|q_{ie}|}, |\omega_i|_{max}\right\} \quad \text{with } d = 2\zeta\omega_n,\ k = 2\omega_n^2$$

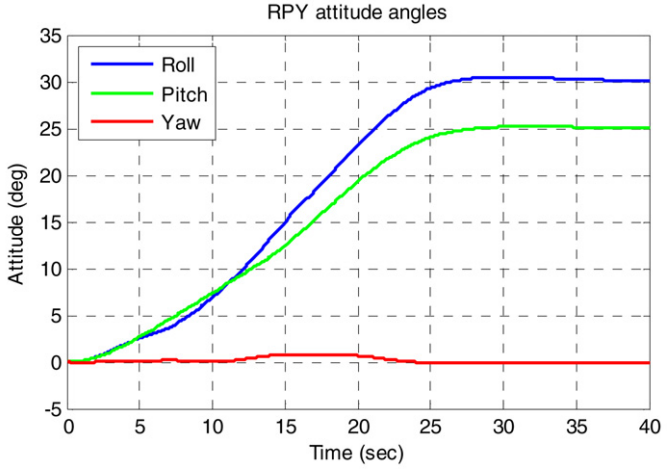

Fig. 9. 4-SGCMG controlled attitude angles from initial gimbal angle vector $\boldsymbol{\delta}(0) = (0, 0, 0, 0)^\circ$.

for $\omega_n = 0.2828$ rad/sec and $\zeta = 0.9$,

$\mathbf{K} = k\mathbf{I} = \text{diag}\{24.0 \quad 24.0 \quad 12.0\}$

$\mathbf{D} = d\mathbf{I} = \text{diag}\{75.0 \quad 75.0 \quad 37.5\}$

$a_i \cong 40\%$ of max control acceleration for axis i

$= \{0.002 \quad 0.002 \quad 0.004\}$ rad/sec^2

$|\omega_i|_{max} = 0.035$ rad/sec $= 2.0\,^\circ$/sec

$\mathbf{N}_{add} =$ Additional torque to uncouple the Euler dynamics

The control law parameter choices in (30) will give a non-saturated 2% settling time of 16 seconds. Finally to adhere to the maximum gimbal rate limit, the reference rate vector is calculated as:

$$\dot{\boldsymbol{\delta}}_{ref} = \operatorname*{sat}_{\pm\dot{\delta}_{\lim}}\left\{\mathbf{A}^{\#}\mathbf{N}_{cmg}\right\} \tag{30}$$

Figs. 9 to 13 show the results of the **RPY** rotation of (26) when the initial 4-SGCMG gimbal angles are all at zero degrees. Fig. 9 shows how the attitude reference angles are reached in approximately 32 seconds, a very similar settling time compared to the NMT dual-wheel system in Fig. 5. However, Fig. 10 indicates higher ORC body angular rates, without the smoothness of the NMT system in Fig. 4. The gimbal angular rates of Fig. 11 clearly show how the rate limit of $\pm 15.0\,^\circ$/sec is constraining the 4-SGCMG control performance, as expected, for an as fast as possible response. Fig. 12 indicates how the final gimbal angles will settle into a zero angular momentum final gimbal vector $(180, 0, -180, 0)^\circ$. Fig. 13 presents the singularity index indicating two periods where internal singularities were encountered and where the GSR steering logic successfully passed through.

Figs. 14 to 16 show the results where the 4-SGCMG system starts initially in the well-known internal elliptic singularity. Fig. 14 shows an increase to approximately 40 seconds for the settling time. Fig. 15 shows how the gimbal angles will not settle into a symmetric and "optimal" configuration for any future maneuvers. The singularity index of Fig. 16 indicates the initial elliptic singularity and how the GSR steering logic manages to escape it within 2 seconds. The overall performance when starting from these initial conditions is clearly not time optimal.

Please cite this article in press as: W.H. Steyn, A dual-wheel multi-mode spacecraft actuator for near-minimum-time large angle slew maneuvers, Aerospace Science and Technology (2008), doi:10.1016/j.ast.2008.01.003

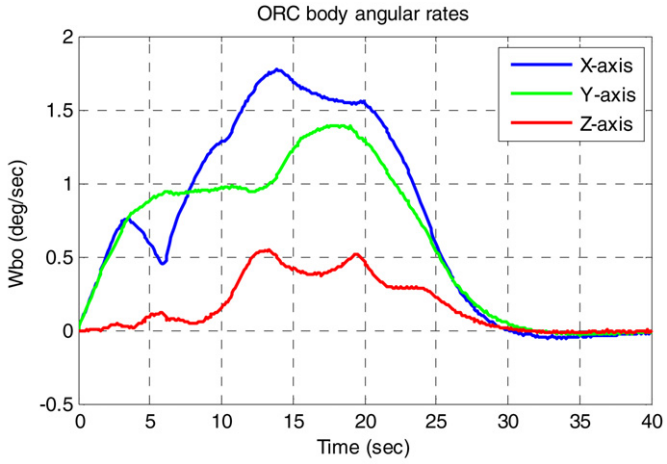

Fig. 10. 4-SGCMG measured body angular rate vector.

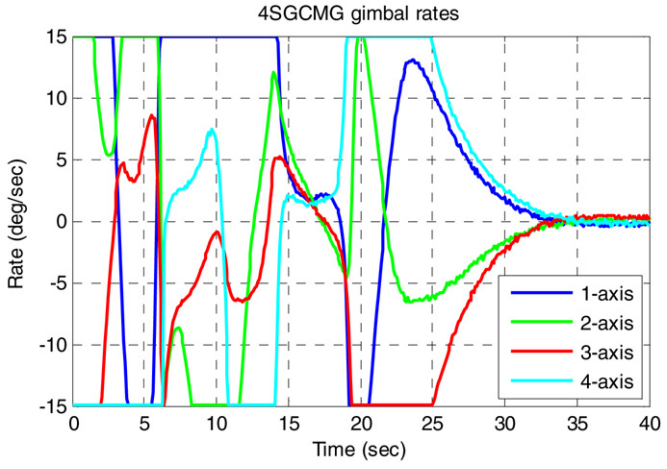

Fig. 11. 4-SGCMG gimbal rates during the maneuver.

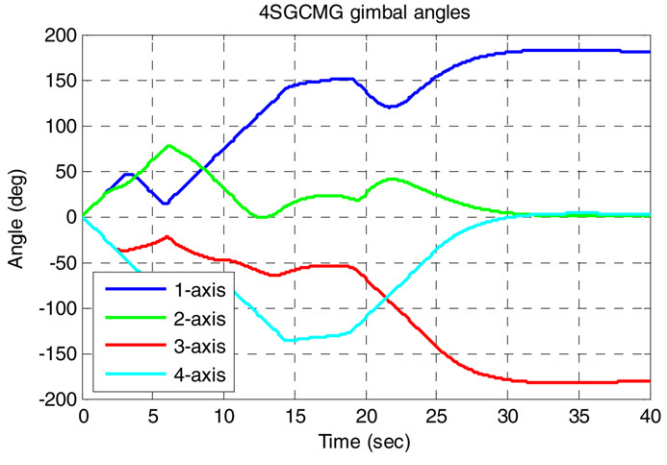

Fig. 12. 4-SGCMG gimbal angles during the maneuver.

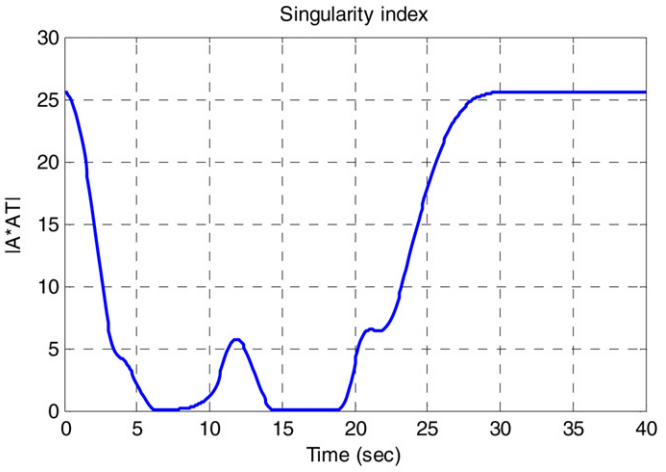

Fig. 13. Singularity index from $\delta(0) = (0, 0, 0, 0)°$.

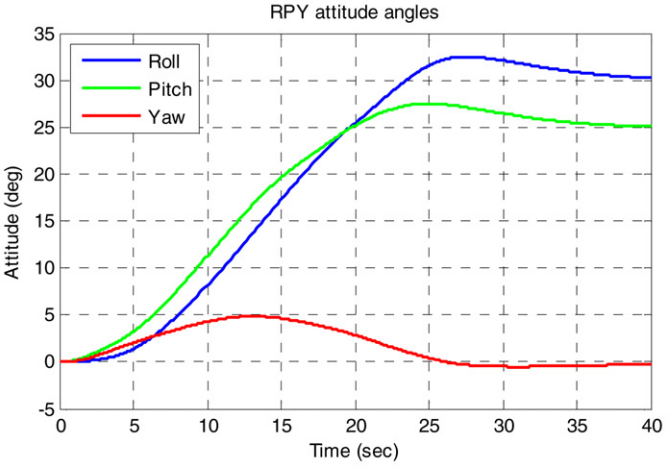

Fig. 14. 4-SGCMG controlled attitude angles from initial gimbal angle singularity vector $\delta(0) = (-90, 0, 90, 0)°$.

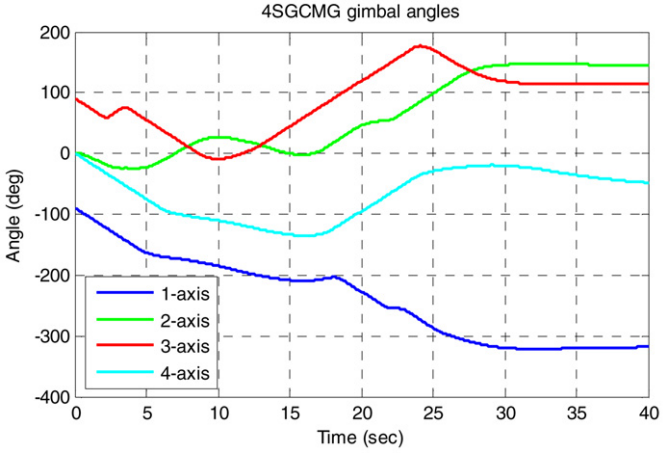

Fig. 15. 4-SGCMG gimbal angles from $(-90, 0, 90, 0)°$.

5. Conclusions

The new dual-wheel actuator implementation presented will be an excellent and cost effective replacement for other wheel actuators in small satellites where high agility and fine stability are required. In CMG-mode, minimum-time slew maneuvers are possible, without the problem of encountering control singularities as prevalent in known gimbal steering control logic as required for other CMG configurations, e.g. the pyramid

Please cite this article in press as: W.H. Steyn, A dual-wheel multi-mode spacecraft actuator for near-minimum-time large angle slew maneuvers, Aerospace Science and Technology (2008), doi:10.1016/j.ast.2008.01.003

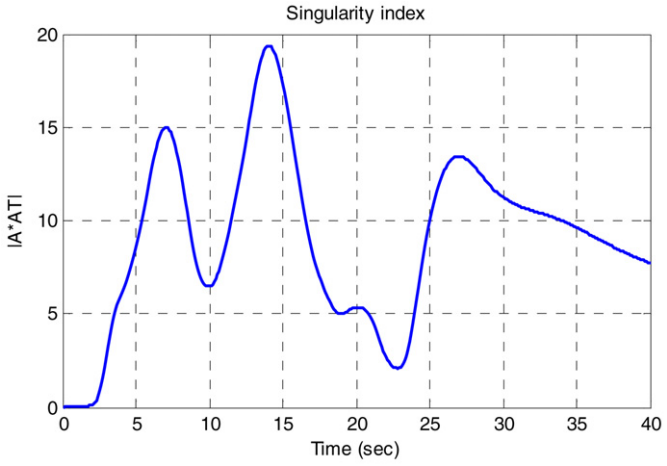

Fig. 16. Singularity index from $\delta(0) = (-90, 0, 90, 0)^\circ$.

4-SGCMG system [4,7,9,13,14]. The peak power requirement during these fast CMG maneuvers is also much lower compared to reaction wheel systems with a similar (or lower) torque capability. A robust, singularity free and computationally simple, NMT eigenaxis rotation controller was presented for the CMG-mode of the dual-wheel system. The NMT eigenaxis CMG-mode controller shows a significant agility improvement to similar sized reaction wheel actuated systems.

The dual-wheel actuator transits smoothly between CMG-mode and RW-mode. For transitions from RW-mode to CMG-mode; if a reaction wheel momentum management system is used to constantly dump any angular momentum build-up (e.g. magnetic torquers), any small angular momentum difference between the wheels per axis can easily be accounted for in the CMG-mode controllers, see Eq. (7). For transitions from CMG-mode to RW-mode; if the gimbal angles are not perfectly zeroed at the end of a large angle maneuver, the RW-mode feedback controller will easily handle a slow open-loop zeroing of the gimbal angles, without any significant disturbances to the satellite's attitude.

Compared to the popular pyramid 4-SGCMG configuration, a smoother and more consistent optimal performance is obtained using the dual-wheel system. Although steering logic exist [7,13] to pass through gimbal singularities, these always come at the expense of degradation in performance. The pyramid 4-SGCMG has one significant advantage in that only four SGCMG units are required, while six SGCMG units are required in the dual-wheel system. The extra mass and power penalty have to be weighed against the obvious advantages of the dual-wheel actuator:

- Predictable response time (no singularities);
- Smooth and symmetric angular momentum and torque profiles;
- CMG and RW application with smooth transition between modes;
- Increased redundancy in case of SGCMG unit failures;
- Control logic with less parameters to tune to optimise the controller performance;
- Simpler mechanical construction of the SGCMG units due to a rotational limit of $\pm 90^\circ$ to the gimbal angles (no slip rings are required).

References

[1] K.D. Bilimoria, B. Wie, Time optimal three-axis reorientation of a rigid spacecraft, AIAA Journal of Guidance, Control, and Dynamics 16 (3) (1993) 446–452.
[2] R.M. Byers, S.R. Vadali, Quasi-closed-form solution to the time-optimal rigid spacecraft reorientation problem, AIAA Journal of Guidance, Control, and Dynamics 16 (3) (1993) 453–461.
[3] J.L. Crassidis, S.R. Vadali, F.L. Markley, Optimal variable structure control tracking of spacecraft maneuvers, AIAA Journal of Guidance, Control, and Dynamics 23 (3) (2000).
[4] J.W. Crenshaw, 2-SPEED, a Single-gimbal control moment gyro attitude control system, in: AIAA Guidance and Control Conference, Aug. 1973, Key Biscayne, Florida, Paper 1973-895, 11 pp.
[5] V. Lappas, W.H. Steyn, C. Underwood, Design and testing of a control moment gyroscope cluster for small satellites, AIAA Journal of Spacecraft and Rockets 42 (4) (2005) 729–739.
[6] F. Li, P.M. Bainum, Numerical approach for solving rigid spacecraft minimum time attitude maneuvers, AIAA Journal of Guidance, Control, and Dynamics 13 (1) (1990) 38–43.
[7] H. Schaub, J. Junkins, Singularity avoidance using null motion and variable-speed control moment gyros, AIAA Journal of Guidance, Control, and Dynamics 23 (1) (2000) 11–16.
[8] W.H. Steyn, Near-minimum-time eigenaxis rotation maneuvers using reaction wheels, AIAA Journal of Guidance, Control, and Dynamics 18 (5) (1995) 1184–1189.
[9] S.J. Thomas, M.A. Paluszek, Architecture for low-power, high-agility multibody control, in: AIAA Infotech@Aerospace, Sept. 2005, Arlington, Virginia, Paper 2005-7041, 15 pp.
[10] S.R. Vadali, Variable-structure control of spacecraft large-angle maneuvers, AIAA Journal of Guidance, Control, and Dynamics 9 (2) (1986) 235–239.
[11] P.P.J. Van den Bosch, W. Jongkind, A.C.M. Van Swieten, Adaptive attitude control for large-angle slew manoeuvres, Automatica 22 (2) (1986) 209–215.
[12] D. Verbin, J.Z. Ben-Asher, Time efficient closed loop steering laws for rigid satellite large rotational maneuver, in: AIAA Guidance, Navigation, and Control Conference, Aug. 2006, Keystone, Colorado, Paper 2006-6042, pp. 1–25.
[13] B. Wie, Singularity escape/avoidance steering logic for control moment gyro systems, AIAA Journal of Guidance, Control, and Dynamics 28 (5) (2005) 948–956.
[14] B. Wie, D. Bailey, C. Heiberg, Rapid multitarget acquisition and pointing control of agile spacecraft, AIAA Journal of Guidance, Control, and Dynamics 25 (1) (2002) 96–104.
[15] B. Wie, H. Weiss, A. Arapostathis, Quaternion feedback regulator for spacecraft eigenaxis rotations, AIAA Journal of Guidance, Control, and Dynamics 12 (3) (1989) 375–380.
[16] T. Zwartbol, R.F. Van den Dam, A.P. Terpstra, P.Th.L.M. Van Woerkom, Attitude estimation and control of a maneuvering spacecraft, Automatica 21 (5) (1985).

Please cite this article in press as: W.H. Steyn, A dual-wheel multi-mode spacecraft actuator for near-minimum-time large angle slew maneuvers, Aerospace Science and Technology (2008), doi:10.1016/j.ast.2008.01.003